Nature Does the Averaging-In-Situ Produced 10Be, 21Ne, and 26Al in a Very Young River Terrace

Andreas Gärtner, Silke Merchel, Samuel Niedermann, Regis Braucher, Team Aster, Peter Steier, Georg Rugel, Andreas Scharf, Loic Le Bras, Ulf Linnemann

geosciences

MDPI

Article

Nature Does the Averaging—In-Situ Produced ^{10}Be, ^{21}Ne, and ^{26}Al in a Very Young River Terrace

Andreas Gärtner [1,2], Silke Merchel [2,3,*], Samuel Niedermann [4], Régis Braucher [5], ASTER-Team [5,†], Peter Steier [6], Georg Rugel [2,3], Andreas Scharf [2], Loic Le Bras [1,7] and Ulf Linnemann [1]

1 Senckenberg Naturhistorische Sammlungen Dresden (SNSD), Museum für Mineralogie und Geologie, Sektion Geochronologie, 01109 Dresden, Germany; andreas.gaertner@senckenberg.de (A.G.); loic.y.lebras@gmail.com (L.L.B.); ulf.linnemann@senckenberg.de (U.L.)
2 Helmholtz-Zentrum Dresden-Rossendorf (HZDR), Institute of Ion Beam Physics and Materials Research, 01328 Dresden, Germany; g.rugel@hzdr.de (G.R.); andreas_scharf@gmx.de (A.S.)
3 Helmholtz-Zentrum Dresden-Rossendorf (HZDR), Helmholtz Institute Freiberg for Resource Technology, 01328 Dresden, Germany
4 Deutsches GeoForschungsZentrum (GFZ), 14473 Potsdam, Germany; nied@gfz-potsdam.de
5 Aix-Marseille Universite, CNRS, IRD, Coll. France, INRAE, CEREGE UM 34, 13545 Aix-en-Provence, France; braucher@cerege.fr (R.B.); bourles@cerege.fr (A.T.)
6 Universität Wien, Fakultät für Physik—Isotopenphysik, 1090 Wien, Austria; peter.steier@univie.ac.at
7 University of the Witwatersrand, School of Geosciences, Johannesburg 2050, South Africa
* Correspondence: s.merchel@hzdr.de
† ASTER Team: Georges Aumaître, Didier Bourlès, Karim Keddadouche.

Received: 2 April 2020; Accepted: 15 June 2020; Published: 18 June 2020

Abstract: The concentrations of long-lived in-situ produced cosmogenic nuclides (^{10}Be, ^{21}Ne, ^{26}Al) in quartz obtained from a very recent (~200 a; based on ^{14}C data on organic material) terrace of the Swakop River in Namibia are nearly constant throughout a 322 cm-long depth profile. These findings corroborate earlier hypotheses postulating a homogeneous distribution of these nuclides in freshly deposited river terrace sediments. An averaged nuclide concentration is a crucial and generally assumed prerequisite for the determination of numerical ages of old sediments.

Keywords: cosmogenic nuclides; accelerator mass spectrometry, dating, river sediments

1. Introduction

Fluvial sediments are excellent archives for terrestrial environments. They record information about palaeoclimate conditions and river catchment areas at the time of their deposition (e.g., [1,2]). The depositional age of such sediments can be determined using in-situ produced cosmogenic nuclides (CN) such as ^{10}Be ($t_{1/2}$ = 1.387 Ma [3,4]), ^{21}Ne (stable), and ^{26}Al ($t_{1/2}$ = 0.705 Ma [5]). Large amounts of some CN, e.g., ^{10}Be and ^{14}C, originate from interactions of cosmic rays with elements in the Earth's atmosphere, particularly nitrogen and oxygen (so-called atmospheric CN). Among the studied nuclides, atmospheric ^{10}Be is adsorbed on aerosol particles and deposited in the sediments via precipitation [6]. In-situ production of ^{10}Be by interaction with minerals in surficial rocks (in-situ ^{10}Be) is several orders of magnitudes lower [7]. In contrast, production of ^{21}Ne and ^{26}Al in the atmosphere is negligible. In-situ production of all CN (^{10}Be, ^{21}Ne, ^{26}Al) is a function of exposure time, altitude, latitude, topographic and self-shielding, and chemical composition of the target mineral [7,8]. In general, the more short-lived CN ^{14}C ($t_{1/2}$ ~5.7 ka [9] and references therein) from in-situ production in quartz can also be used for dating [10,11]. However, more often (and also in this study) ^{14}C produced in the atmosphere, incorporated in equilibrium in organic materials and buried in sediment layers, is used for indirect dating [12,13].

Ephemeral river systems like the Swakop River of Namibia occur in arid regions worldwide. Thus, these rivers play a major role in basin drainage and sediment transport [14,15]. Their siliciclastic deposits are valuable archives that are widely used to understand landscape evolution and transport processes [16–18].

Several studies postulate an averaged in-situ CN signal in freshly deposited riverine sediments, soils, or regolith due to mixture of mineral grains with different pre-exposure histories [19,20]. Thus, uniform CN concentrations (due to high CN concentrations from inheritance) in depth profiles from such sediments indicate very young, i.e., Mid to Late Holocene, deposition ages [21]. This is consistent with the common phrase that "nature does the averaging" [22,23], which is the inevitable prerequisite for dating river terraces of any age.

The current detection limit of accelerator mass spectrometry (AMS) and noble gas mass spectrometry methods, and the extremely low CN concentrations resulting from in-situ production, restrict the lower age limit to about one to a few hundred years [24–26]. Hence, dating of very young fluvial deposits can be challenging. This also applies for the depth profile from a location close to the lower Swakop River (Namibia) investigated here. As the denudation in the entire Swakop catchment is known to be remarkably low and homogeneous [27,28], consideration and discussion of potentially variable denudation rates is not a subject of great concern. Thus, the sampled ephemeral river sediments represent an ideal archive concerning the aim of this study. The sedimentological features of the studied profile resemble those of profiles upstream from the presented locality, which are only a few hundred years old (see Section 2 for details). Therefore, this study only aims to provide evidence for the yet postulated averaging of the CN signal at the time of sedimentation [19] for ^{10}Be, ^{21}Ne, and ^{26}Al in a very young river terrace, even for ephemeral conditions. However, accurate numerical age determination of such profiles requires more suitable dating techniques like radiocarbon age determination of organic material (if present).

2. Location and Geological Setting

The Swakop River is among the largest ephemeral rivers of Namibia and drains a catchment area of 30,100 km^2 with an elevation range of zero to 2479 m a.s.l.. In contrast to perennial river systems, sediment deposition is dependent on the amount of regional precipitation, and therefore stochastic on small time scales. Beside the phases of Latest Pleistocene to Holocene sediment accumulation, the fluvial record of the Swakop River reaches back to the possibly Upper Oligocene "Langer Heinrich Formation" [29]. These sediments fill a palaeovalley, which is now used by the Tumas River. Due to the significant occurrence of uraniferous gravels, the sedimentology and stratigraphy of this succession is well-documented [30,31]. The "Langer Heinrich Formation" is unconformably overlain by fluvial facies of most likely Lower Miocene "Tsondab Sandstone Formation" [29,31]. The whole succession is discordantly covered by conglomerates of the "Karpfenkliff Formation", which is assumed to have a mid- or upper Miocene age [29,31,32]. Remnants of Pliocene strata could not yet be found in this area [29]. All of these pre-Pleistocene terrace complexes occur south of the modern Swakop River course (Figure 1b), indicating a northward migration of the river through time. The adjacent Kuiseb River valley hosts the well-studied upper Pleistocene "Homeb Silts" [33,34] and the uppermost Pleistocene "Gobabeb Gravel Formation" [29,35]. Possibly equivalent deposits are also known from the middle and upper reaches of the Swakop River and some of its tributaries [29,36].

The Swakop River and its tributaries drain large parts of the southern Damara Belt, which has a complex geology and comprises various rock types of mostly Cryogenian-Cambrian age (Figure 1a, see legend for time scale) [37]. The Palaeo- to Mesoproterozoic Abbabis Gneiss Complex forms an inlier within the central parts of the orogen [38]. However, there is also a younger cover sequence formed by siliciclastic and igneous rocks [39]. Detailed descriptions are given elsewhere [40,41] and references therein. The vast majority of the rocks in the mentioned geologic units contain quartz, which suggests an equal delivery of the latter from the entire catchment area.

Quartz-rich sediment samples were collected in January 2015 in a sporadically mined sand and gravel pit close to the ephemeral Swakop River, Namibia (22.64069° S, 14.67411° E, 90 m a.s.l., Figure

1c), from a 322 cm-long depth profile consisting of intercalated coarse-grained, plane bedded sand and fine to coarse gravel (Figure 2a). These sediments belong to the lowermost terrace complex of the Swakop River. According to time-resolved Google Earth satellite image series, the profile at one wall of the sand and gravel pit was exhumed after October 2013. This recent excavation has a constant depth of more than three metres and a large lateral extent of more than 80 m, which makes this profile an ideal site for sedimentological and cosmogenic nuclide depth profile studies as well as for testing the hypothesis that "nature does the averaging" *sensu* earlier works [22,23].

Three of the recorded gravel layers can be traced for several tens of metres, while the others are a few centimetres thin and of limited extent. This gives reason to assume that at least three flood events led to sediment deposition, matching with records of flood recurrence in the past millennium from the lower reaches of the Khan River and the middle reaches of the Swakop River [42]. There, several layers of flood deposits—from about 35 individual events—including gravel layers were dated between 240 ± 90 a and 90 ± 20 a using optically stimulated luminescence (OSL) [42]. Flood-derived coarse gravels with apparent ages between 350 and 100 years BP are also known from the Swakop River's mouth [43]. Below 300 cm depth, the sediments gradually become calcified, resulting in solidification at about 322 cm. Additionally, changing sediment colour and an older erosion surface on top of the calcified sediments (likely formed by the first of the three floods) led to the assumption that the deposits below a depth of 322 cm are a separate, older sediment complex originating from an earlier series of flood events. Older phases of extensive sediment deposition, mainly coarse sands, with OSL ages between 5100 ± 620 a and 14,900 ± 1700 a, followed by intensive calcification, have been found at other sites along the entire Swakop River catchment [42,43].

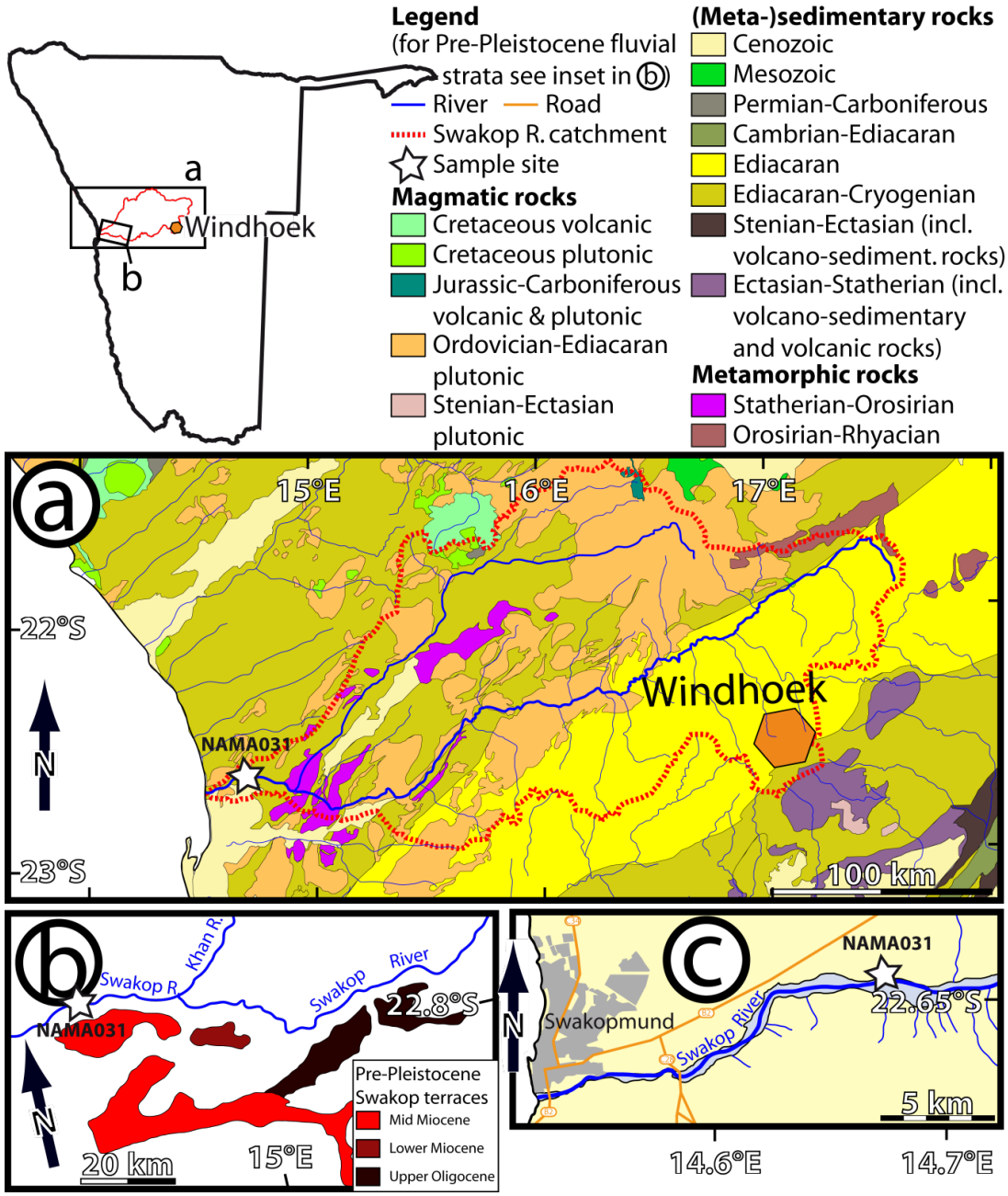

Figure 1. Geographic and geological overview of the study area and sampling site. (**a**) Geological map of the Swakop River catchment and its surrounding areas adapted from [44]. (**b**) Mapped Pre-Pleistocene terraces along the southern banks of the Swakop River [29] and references therein. (**c**) Sample locality of NAMA031 at the northern banks of the Swakop River east of Swakopmund.

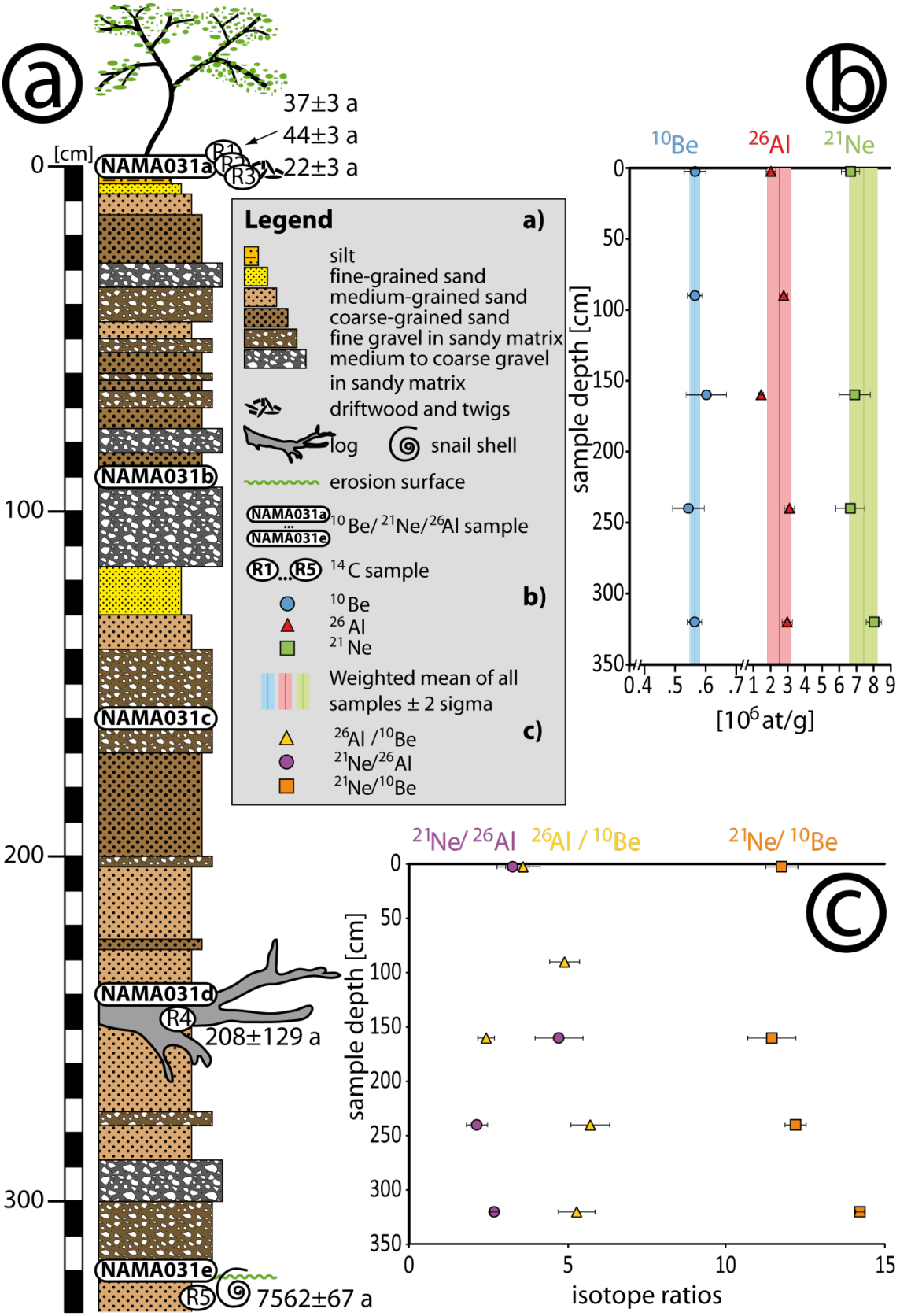

Figure 2. (**a**) Stratigraphic column of profile NAMA031 and carbon-14 ages (for R1–R5). (**b**) Depth-related CN concentrations (for NAMA031a to NAMA031e), mean and 2 sigma uncertainty of CN along the profile. (**c**) Isotope ratios versus sample depth at the 2 sigma level.

3. Materials and Methods

Five sediment samples of sand or sandy matrix of gravelly layers were taken in 2015 at profile depths of 0–5, 87–93, 158–162, 237–243, and 318–322 cm, respectively (NAMA031a, NAMA031b, NAMA031c, NAMA031d, NAMA031e). They were all analysed for their ^{10}Be, ^{26}Al, and—except for sample NAMA031b—^{21}Ne concentrations. Radiocarbon ages of driftwood and twigs (R1, R2, R3) from three accumulations of organic material in the topmost 15 cm of the profile, a piece of wood from a log found in the lower part of the sedimentary package (R4, about 60 m to the SE of the depth profile), and a snail shell (R5) from the top of the older sediment complex, all sampled in 2016, were used to bracket the age of the sediments.

The samples for ^{14}C analysis were prepared at the sample preparation unit for small samples for environmental research and medicine at the University of Vienna, Vienna Environmental Research Accelerator (VERA) facility [45]. Wood samples (R1–R4) were exposed to the standard acid-base-acid treatment and combusted in closed quartz vials. The snail shell sample (R5) was converted to CO_2 by hydrolysis with H_3PO_4. Considering the small sample size and the possible incorporation of carbonate by the living snail [46], a pre-etching step was omitted. The age obtained may thus represent an upper limit. Samples were normalised to IAEA-C3 cellulose, IAEA-C2 carbonate, and the VERA in-house-standard Vienna-CTW2 (graphite, Fraction Modern $F^{14}C$ = 1.254 ± 0.005) and blank-corrected using IAEA-C1 (carbonates) and the in-house-standard Vienna-HPG (wood samples). Calibration was performed with OxCal v4.3.2, calibration curves INTCAL 13 and BOMB 13 NH1.

Enrichment of 200–1000 μm quartz grains ($\varrho \approx 2.65$ g/cm^3) from the polymineral samples required a two-stage separation process: 1.) Density separation using lithiumheteropolytungstate in water at densities of 2.60 and 2.70 g/cm^3. 2.) Hand-picking under a binocular microscope (ZEISS Stemi-2000) to exclude quartz with interior non-quartz mineral inclusions. Further steps were carried out in a dedicated CN laboratory to remove residual non-quartz-minerals. The quartz concentrate was cleaned with a 1:1 solution of H_2SiF_6 (35%) and HCl (32%) in three (NAMA031a & NAMA031b) and five steps (NAMA031c, NAMA031d, NAMA031e), respectively [47]. Beryllium-10 from production in the atmosphere was removed by three consecutive dissolution steps of the surfaces with 48% HF, resulting in ca. 10% mass loss of the quartz grains per step. Solid aliquots for ^{21}Ne analysis were taken prior to total dissolution of quartz in 48% HF. Two processing blanks for radionuclide analysis were added to monitor all possible unwanted contributions such as contamination between samples in the chemistry lab and during measurement, and from all chemical products and target preparation materials used. All samples and the blanks were processed with ca. 300 μg of a ^{9}Be carrier ("Phenakite DD"; ~0.1 g solution with a ^{9}Be concentration of 3025 ± 9 μg/g [48]) and ca. 900 μg of a commercial ^{27}Al carrier (Carl Roth GmbH, Karlsruhe, Germany; ca. 0.9 g solution with a ^{27}Al concentration of 1000.5 ± 2.0 mg/L; ϱ = 1.011 g/cm^3). Further chemical separation of Be and Al followed the procedures described in [49]. Determination of natural ^{27}Al was done via inductively coupled plasma mass spectrometry (ICP-MS; iCAP RQ, Thermo Fisher: Waltham, MA,USA) of representative aliquots (2.6–2.9 weight % of the sample). Resulting BeO and Al_2O_3 were mixed with Nb (ca. 4 × mass of BeO) and Ag powder (ca. 1 × mass of Al_2O_3), respectively. Both mixtures were pressed into Cu cathodes.

The ^{10}Be/^{9}Be and ^{26}Al/^{27}Al ratios of each sample and the two blanks were determined either at the Dresden Accelerator Mass Spectrometry (DREAMS) facility [50] or at the Accélérateur pour les Sciences de la Terre, Environnement, Risques (ASTER) facility at Centre Europeéen de Recherche et d'Enseignement des Géosciences de l'Environnement (CEREGE) [51]. Results were all quantified versus the in-house standards SMD-Be-12 (^{10}Be/^{9}Be = 1.704 ± 0.030 × 10^{-12}) [50] and SMD-Al-11 (^{26}Al/^{27}Al = 9.66 ± 0.14 × 10^{-12}) [52]. Full details of AMS measurement procedures can be found elsewhere [50–52].

For cosmogenic ^{21}Ne determination in quartz samples NAMA031a, NAMA031c, NAMA031d, and NAMA031e at GFZ Potsdam, ca. 0.7 g of cleaned quartz were degassed by stepwise heating (400, 600, 800, 1200 °C) and analysed according to procedures described in [53]. In addition, aliquots of

approximately 1 g of all samples except NAMA031c were vacuum-crushed to reveal non-atmospheric and non-cosmogenic trapped ^{21}Ne components [54].

4. Results

Results are summarised in Tables 1–3 and Figure 2. Carbon-14 results gave ages between 208 ± 129 a (R5) and 7562 ± 67 a (R4), while the topmost samples yielded 44 ± 3 a (R2), 37 ± 3 a (R1), and 22 ± 3 a (R3) (Table 3, Figure 2a).

Measured ^{10}Be concentrations for all samples overlap within 1 sigma uncertainties throughout the profile and range from 5.44 ± 0.26 × 10^5 to 6.03 ± 0.33 × 10^5 at/g. Three of the five ^{26}Al values (NAMA031b, NAMA031d, NAMA031e) are statistically indistinguishable within 2 sigma, ranging between 2.77 ± 0.24 × 10^6 and 3.11 ± 0.30 × 10^6 at/g. The surface sample NAMA031a contains slightly less (~30%, i.e., 2.03 ± 0.14 × 10^6 at/g) ^{26}Al, which further applies even more for sample NAMA031c (1.46 ± 0.07 × 10^6 at/g). Hence, the ^{26}Al/^{10}Be ratios for samples NAMA031b, NAMA031d and NAMA031e are the same within 2 sigma uncertainties, whereas the ^{26}Al/^{10}Be ratios of NAMA031a and NAMA 031c would overlap with sample NAMA031b within their 3 sigma and 7 sigma errors, respectively. The four ^{21}Ne samples NAMA031a, NAMA031c, NAMA031d and NAMA031e show the same trend as the ^{10}Be signal, although the total ^{21}Ne excess in the 400–800 °C heating steps, usually assumed to be cosmogenic, is 20% higher in NAMA031e. This could be a result of an increased amount of nucleogenic ^{21}Ne in this sample (Figure 3); high concentrations of He with radiogenic isotopic composition (Table 3) support an important contribution of nucleogenic Ne.

Table 1. Radiocarbon data for wood and snail samples. The time ranges of the calibrated ages correspond to 68.2% probability.

Sample	Sample Material	VERA ID	Fraction Modern	Calendar Age (BC/AD)		
			$F^{14}C$ ± 1 sigma	**from**	**to**	**%**
R1	driftwood	VERA-51821	1.271 ± 0.012	1978	1983	68.2
R2	driftwood	VERA-51822	1.415 ± 0.017	1973	1978	68.2
R3	driftwood	VERA-51823	1.128 ± 0.008	1992	1998	68.2
R4	massive log of a tree	VERA-51824	0.984 ± 0.010	1680	1763	26.8
				1802	1893	30.8
				1906	1938	10.6
R5	snail	VERA-51825	0.441 ± 0.004	−5611	−5591	10.7
				−5565	−5478	57.5

Table 2. Sample information and radionuclide data [1]. AMS data for NAMA031a,b,e (and Blank a,b,e) measured at DREAMS and for NAMA031c,d (and Blank c,d) measured at ASTER, respectively. Bulk rock density is 2.33 g/cm^3 for all samples.

Sample Name	Sample Depth [cm]	Sample Thickness [cm]	Mean Depth [cm]	^{10}Be/^{9}Be [10^{-13}]	^{10}Be [10^5 at/g]	^{26}Al/^{27}Al [10^{-13}]	^{27}Al (by ICP-MS) [µg/g]	^{26}Al [10^6 at/g]	^{26}Al/^{10}Be
NAMA031a	0–5	5	2.5	7.55 ± 0.24	5.66 ± 0.18	1.82 ± 0.11	466 ± 14 [2]	2.03 ± 0.14	3.59 ± 0.27
NAMA031b	87–93	6	90	13.89 ± 0.29	5.65 ± 0.12	7.75 ± 0.26	142.4 ± 4.3	2.77 ± 0.12	4.90 ± 0.24
NAMA031c	158–162	4	160	13.02 ± 0.71	6.03 ± 0.33	3.94 ± 0.14	166.3 ± 5.0 [2]	1.46 ± 0.07	2.42 ± 0.18
NAMA031d	237–243	6	240	11.80 ± 0.56	5.44 ± 0.26	7.92 ± 0.30	175.9 ± 5.3	3.11 ± 0.15	5.72 ± 0.39
NAMA031e	318–322	4	320	13.66 ± 0.30	5.64 ± 0.12	5.36 ± 0.21	230.6 ± 6.9	2.98 ± 0.15	5.28 ± 0.29
Blank NAMA031a,b,e				0.0159 ± 0.0039		0.067 ± 0.049	not measured (carrier)		
Blank NAMA031c,d				0.0179 ± 0.0046		0.012 ± 0.012	not measured (carrier)		

[1] Total uncertainties at 1 sigma are derived from counting statistics and uncertainties of the standards summing up to 3.0–11.0% (^{10}Be) and 3.9–6.7% (^{26}Al), respectively. Further uncertainties result from blank correction and for ^{26}Al from uncertainty of ^{27}Al ICP-MS analysis (^{10}Be 2.1–4.9%, ^{26}Al 4.4–6.7%) and stable isotope carriers (^{9}Be 0.3%, ^{27}Al 0.2%). [2] Might be erroneous due to non-quantitative destruction of secondary precipitate (see Section 5).

Table 3. He and Ne data. Uncertainties are 2 sigma.

Sample Name / Weight [g]	T [°C]	^{4}He [10^{-8} cm^3 STP/g]	^{20}Ne [10^{-12} cm^3 STP/g]	^{3}He/^{4}He [10^{-6}]	^{22}Ne/^{20}Ne [10^{-2}]	^{21}Ne/^{20}Ne [10^{-2}]	^{21}Ne$_{ex}$ [a] [10^{6} at/g]
NAMA031a 0.70486	400	3.73 ± 0.19	26.0 ± 1.5	$0.019^{+0.042}_{-0.019}$	10.26 ± 0.16	0.478 ± 0.043	0.80 ±0.33
	600	126.6 ± 6.3	30.7 ± 1.8	0.0069 ± 0.0029	10.74 ± 0.16	0.869 ± 0.029	4.17 ±0.34
	800	323 ± 16	24.6 ± 1.5	0.0018 ± 0.0018	10.34 ± 0.24	0.620 ± 0.028	1.67 ±0.23
	1200	235 ± 12	3.55 ± 0.53	$0.0016^{+0.0026}_{-0.0016}$	10.90 ± 0.25	6.59 ± 0.82	5.941 ± 0.45
	Total	688 ± 21	84.9 ± 2.8	0.0028 ± 0.0014	10.48 ± 0.10	0.916 ± 0.054	6.66 [b] ± 0.53
NAMA031c 0.71046	400	11.97 ± 0.84	44.6 ± 5.7	$0.019^{+0.023}_{-0.019}$	10.51 ± 0.23	0.585 ± 0.041	2.65 ± 0.61
	600	129.8 ± 9.1	24.8 ± 3.3	$0.0045^{+0.0065}_{-0.0045}$	10.44 ± 0.42	0.749 ± 0.065	2.56 ± 0.54
	800	223 ± 11	30.9 ± 2.1	<0.0037	10.61 ± 0.24	0.569 ± 0.044	1.70 ± 0.40
	1200	120.5 ± 6.0	4.44 ± 0.68	$0.0015^{+0.0057}_{-0.0015}$	13.38 ± 0.90	5.02 ± 0.93	5.55 ± 0.89
	Total	485 ± 16	104.7 ± 6.9	$0.0020^{+0.0057}_{-0.0020}$	10.64 ± 0.16	0.807 ± 0.056	6.91 [b] ± 0.91
NAMA031d 0.70614	400	3.57 ± 0.21	23.2 ± 1.5	$0.022^{+0.009}_{-0.022}$	10.68 ± 0.26	0.457 v 0.045	0.58 ± 0.30
	600	109.0 ± 6.5	32.5 ± 2.0	0.0083 ± 0.0064	10.66 ± 0.26	0.887 ± 0.061	4.56 ± 0.60
	800	334 ± 20	35.1 ± 2.3	$0.0011^{+0.0040}_{-0.0011}$	10.60 ± 0.23	0.525 ± 0.050	1.51 ± 0.50
	1200	160.2 ± 9.6	3.71 ± 0.72	$0.0039^{+0.0068}_{-0.0039}$	12.80 ± 0.99	4.1 ± 1.0	3.73 ± 0.84
	Total	607 ± 23	94.5 ± 3.5	0.0033 ± 0.0031	10.70 ± 0.14	0.773 ± 0.056	6.65 [b] ± 0.84
NAMA031e 0.70594	400	17.27 ± 0.87	39.9 ± 2.5	$0.007^{+0.011}_{-0.007}$	10.65 ± 0.15	0.779 ± 0.011	4.46 ± 0.32
	600	116.4 ± 5.8	23.4 ± 1.6	$0.0005^{+0.0022}_{-0.0005}$	10.26 ± 0.19	0.762 ± 0.029	2.50 ± 0.25
	800	174.3 ± 8.8	16.7 ± 1.3	$0.0010^{+0.0055}_{-0.0010}$	10.02 ± 0.24	0.602 ± 0.035	1.07 ± 0.18
	1200	84.9 ± 4.2	1.22 ± 0.46	$0.0004^{+0.0020}_{-0.0004}$	10.0 ± 4.0	10.0 ± 3.7	3.15 ± 0.43
	Total	393 ± 11	81.2 ± 3.3	$0.0010^{+0.0026}_{-0.0010}$	10.40 ± 0.12	0.876 ± 0.077	8.03 [b] ± 0.44
NAMA031a 1.00426	Crush	1.435 ± 0.072	98.0 ± 7.2	0.16 ± 0.11	10.20 ± 0.13	0.363 ± 0.018	-
NAMA031d 1.00680	Crush	2.33 ± 0.12	62.0 ± 4.6	$0.051^{+0.066}_{-0.051}$	10.28 ± 0.19	0.407 ± 0.029	-
NAMA031e 1.07402	Crush	2.23 ± 0.11	66.6 ± 3.5	0.058 ± 0.046	10.19 ± 0.11	0.3607 ± 0.0084	-

[a] Excess ^{21}Ne relative to a trapped Ne isotopic composition as determined in the crusher extractions (bottom of table). For the trapped ^{21}Ne/^{20}Ne ratio, a weighted mean of 0.00364 ± 0.00015 was used for all samples. [b] Sum of 400–800 °C steps, which is assumed to correspond to total cosmogenic ^{21}Ne [55].

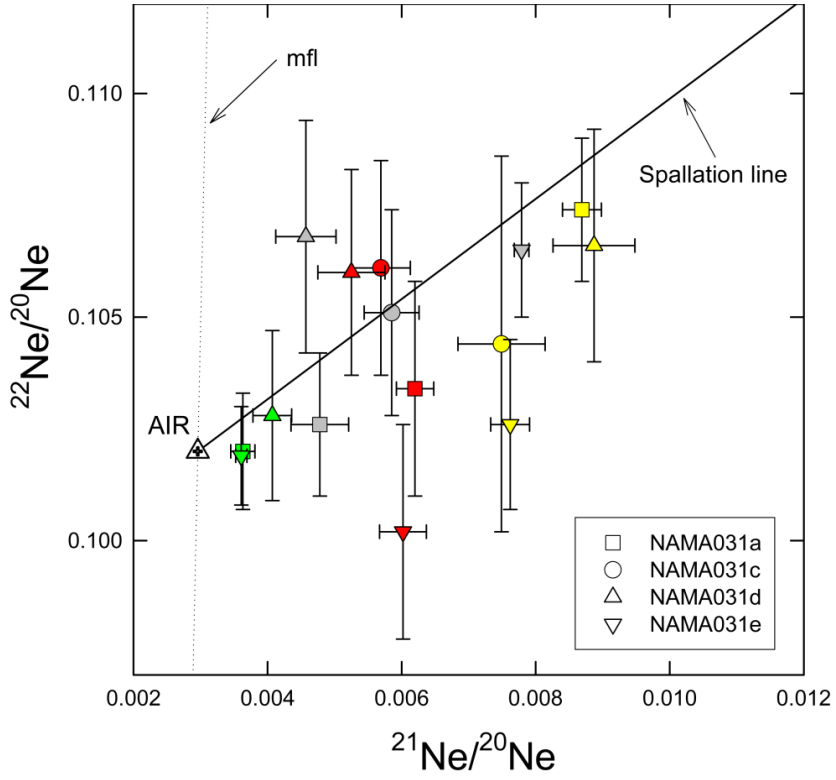

Figure 3. Neon three-isotope plot for stepwise heating and crushing data of NAMA031a, NAMA031c, NAMA031d and NAMA031e (grey—400 °C, yellow—600 °C, red—800 °C, green—crushing extractions). The 1200 °C data would plot out of scale far to the right (see Table 2). "Spallation line", i.e., mixing line of atmospheric and cosmogenic Ne, according to [56]. mfl: mass fractionation line. While the NAMA031a, NAMA031c and NAMA031d data are consistent with a two-component mixture of trapped Ne (as determined by the crusher extractions) and cosmogenic Ne, the 600 °C and 800 °C steps of NAMA031e may indicate the presence of some nucleogenic ^{21}Ne in addition. 2 sigma uncertainties are shown.

5. Discussion

The maximum age of the investigated terrace complex is given by a (calibrated) ^{14}C age of 7562 ± 67 a obtained from the snail shell (R5) on top of the calcified sands (lowermost part of the profile, Figure 2a). This age is in line with the termination of widespread calcrete formation and palaeoflood events in the Swakop catchment at 8.8 ± 1.0 ka [42,43]. The evaluation of different palaeoclimate proxies all over Namibia led to the assumption of much wetter conditions during the Early Holocene, which caused significantly higher runoff than today [57]. Just after the Early to Mid-Holocene transition, the climate of southern Africa became much drier [58], resulting in a decreased discharge and a lack of flood-derived sediments in the Swakop River [42]. Accordingly, the age of the snail shell (R5) allows the determination of the stratigraphic position of the sediments below the Swakop River's youngest terrace complex.

However, the unconsolidated sands that were sampled are likely much younger. An apparent ^{14}C age of 208 ± 129 a was calculated for the sampled tree log (R4), which times the formation of the lower part of the unconsolidated sand and gravel sequence. This age fits with the increased number of flood events between ca. 1450 and ca. 1800 AD throughout Namibia [42,43,59,60]. The latter interval is almost coeval to the Little Ice Age that is characterised by globally cooler climate conditions with wet and dry periods in southern Africa [61]. At least northeastern Namibia received significantly higher precipitation than today in the decades around 1800 AD [61]. The apparent absence of sediments from the period between ca. 7000 and 400 a shows a striking similarity to parts of the adjacent Kuiseb River [59]. This underlines the possibility of exceptionally high discharge at about 400 a [61], possibly eroding and reworking the older sediments [59].

The youngest ^{14}C ages result from twig and driftwood samples R1 (37 ± 3 a), R2 (44 ± 3 a), and R3 (22 ± 3 a). They may represent remnants of minor floods (e.g., in 1972, 1974, 1976, 1984 [42,62]) that post-date the main sediment accumulation at the studied site and that mirror decreasing runoff caused by increasing aridity since about 1800 AD [42,57,63].

Except for the slightly lower ^{26}Al concentrations of the surface sample NAMA031a and of sample NAMA031c, the entire profile exhibits a homogenous CN concentration with similar $^{26}Al/^{10}Be$ ratios. This supports the hypothesis of homogenised CN signals in very young fluvial deposits, at least for ephemeral river systems. Hence, essentially the entire production of the studied long-lived CN must have occurred during pre-exposure and/or sediment transport, while the in-situ production of CN after sediment deposition is negligible. Considering a maximum deposition age of 400 a, a Sea Level High Latitude (SLHL) production rate for ^{10}Be of 4.02 at/(g a) [64] scaled using [65] and no additional correction like topographic or self-shielding for "after-deposition production" yielded maximum ^{10}Be and ^{26}Al surface concentrations of ca. 1800 and 11,700 at/g, respectively, which is far lower than the measured concentrations. This is further corroborated by $^{26}Al/^{10}Be$ ratios in a range of 2.42 ± 0.13 to 5.72 ± 0.31, which are depleted with respect to the production rate of 6.61 ± 0.52 [66] and indicate that the quartz grains must have been exposed to cosmic rays at the surface a long time before their deposition in the terrace. The same applies for the $^{21}Ne/^{26}Al$ and $^{21}Ne/^{10}Be$ ratios (Figure 2c).

An explanation of what can be observed in this restricted outcrop can be deduced from earlier published data of the Swakop River's catchment area and the adjacent regions. This allows a better documentation of average CN concentrations that can be found in this part of Namibia. To do so, we have taken benefit of the work of Bierman and Caffee [27], where 66 samples were prepared for both ^{10}Be and ^{26}Al measurements. Ignoring the ten northern samples (samples NAM-52 to NAM-62) due to their remote distance to the studied area, there is a good agreement between the CN concentrations of this study and those of [27] (Figure 4). Additionally, no correlation to altitude can be observed. As mentioned in [27], our study confirms that small streams are eroding more rapidly than surrounding outcrops.

Although only five samples were taken at the site discussed here, at least the ^{10}Be signal is completely averaged throughout the profile. This also holds for ^{21}Ne and ^{26}Al (except for NAMA031c ^{26}Al) when considering the weighted mean of all samples ± 2 sigma. This applies for four (out of five) of the ^{26}Al, as well as for all four investigated ^{21}Ne samples (Figure 2b), which excludes different provenances of quartz grains from NAMA031a to NAMA031e.

The lower ^{26}Al values of the surface sample NAMA031a and sample NAMA031c might be partially explained by erroneous ^{27}Al data, likely caused by the formation of "aluminium-magnesium-fluorides (xH_2O)", which have been produced as secondary reaction products during the sample digestion [67]. Total destruction of these compounds is challenging for some sample compositions (high in Mg) and sometimes does not allow quantitative redissolution of aluminium for accurate ^{27}Al determination in liquid aliquots. Regrettably, we have not analysed the aliquots for Mg concentrations to have final proof, however, the measured ^{27}Al concentration, being two to three times higher in NAMA031a than in the other two samples (Table 1), is usually a well-accepted proxy also for a high Mg concentration [47].

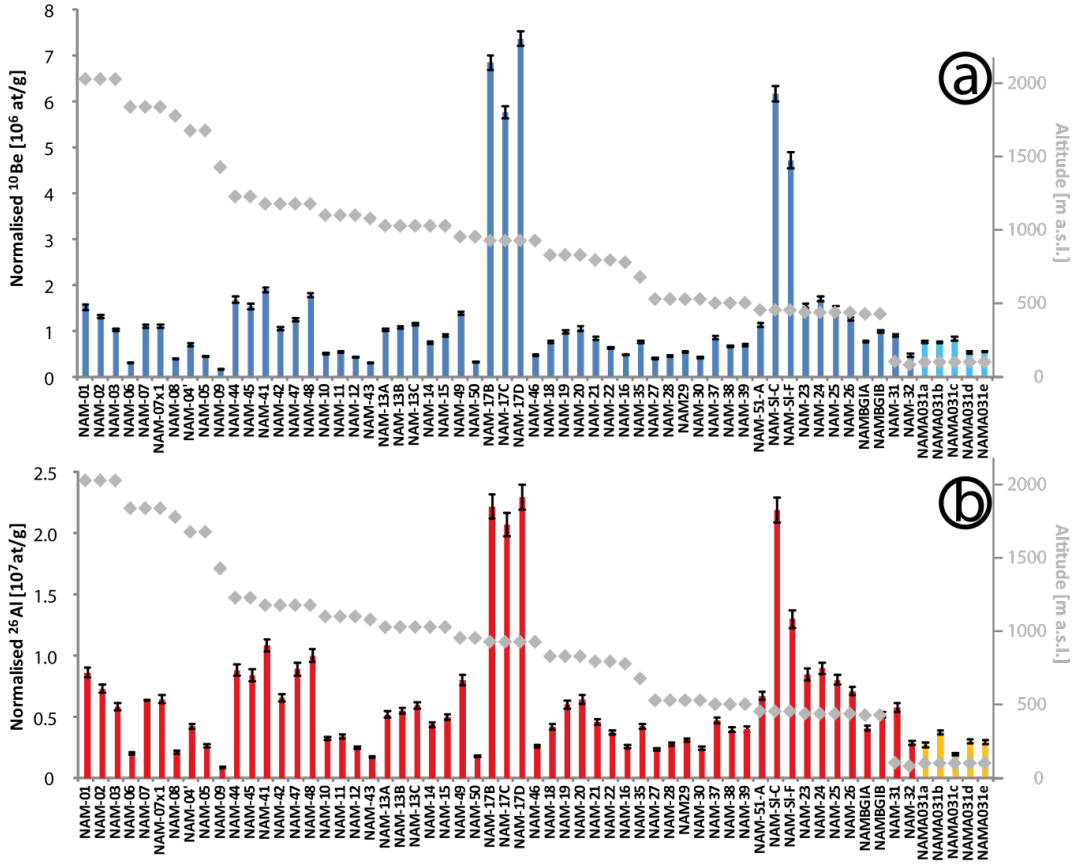

Figure 4. Normalised (**a**) ^{10}Be and (**b**) ^{26}Al concentrations versus altitude of the sample location in samples of [27] and from this study (the five rightmost samples of panels a and b, i.e., NAMA031 a-b-c-d-and e).

6. Conclusions

Radiocarbon ages of organic materials time the terminal deposition of an older terrace complex at 7562 ± 67 a, while the deposition of the studied part of the profile is about 200 years old or even younger. These ages are in line with the increased flood frequency at the terminal phase of calcrete formation in the Early Holocene and during the Little Ice Age.

The studied profile gives evidence for a complete averaging of long-lived and stable CN concentrations in young, i.e., Latest Holocene fluvial sediments. Negligible in-situ production of those CN since deposition indicates that the measured signal is mostly inherited from previous exposure. These data strongly support the hypothesis that "nature does the averaging" by complete and homogeneous mixing of the sediments before and during deposition. Additional proof for sediment supply representative of the entire catchment area of the Swakop River and not biased by a single dominant source is given by detrital zircon data, which indicate the presence of material from all major lithological units [68].

Author Contributions: Conceptualization, A.G., S.M.; Methodology, A.G., S.M.; Validation, R.B., S.N., G.R., P.S.; Formal Analysis, R.B., S.M., S.N., G.R., P.S.; Investigation, A.G., L.LB., S.M., S.N., G.R., A.S., P.S., A.-T.; Resources, R.B., U.L., S.M., S.N., P.S.; Data Curation, R.B., A.G., S.M., S.N., G.R., P.S.; Writing—Original Draft Preparation, A.G.; Writing—Review & Editing, R.B., A.G., S.M., S.N., P.S.; Visualization, A.G.; Supervision, A.G., U.L., S.M.; Project Administration, A.G., U.L.; Funding Acquisition, U.L., S.M.. All authors have read and agreed to the published version of the manuscript.

Funding: This research was funded by the Deutsche Forschungsgemeinschaft (DFG), Project LI 521/32-1.

Acknowledgments: Parts of this research were carried out at the Ion Beam Centre (IBC) at the Helmholtz-Zentrum Dresden-Rossendorf e. V., a member of the Helmholtz Association. We would like to thank the DREAMS operator team for their assistance with AMS measurements. The ASTER AMS national facility

(CEREGE, Aix-en-Provence) is supported by the INSU/CNRS, the ANR through the "Projets thématiques d'excellence" program for the "Equipements d'excellence" ASTER-CEREGE action and IRD. Furthermore, the authors like to thank R. Krause, M. Hofmann, J. Zieger, M. Stutzriemer, J. Harazim, and J. Rothe for field assistance and help during quartz picking, E. Schnabel for performing the noble gas analyses and S. Beutner for ^{27}Al analysis by ICP-MS.

Conflicts of Interest: The authors declare no conflict of interest.

References

1. Von Suchodoletz, H.; Gärtner, A.; Hoth, S.; Umlauft, J.; Sukishvili, L.; Faust, D. Late Pleistocene river migrations in response to thrust belt advance and sediment-flux steering—The Kura River (southern Caucasus). *Geomorphology* **2016**, *266*, 53–65, doi:10.1016/j.geomorph.2016.04.026.
2. Gärtner, A.; Linnemann, U.; Hofmann, M. The provenance of northern Kalahari Basin sediments and growth history of the southern Congo Craton reconstructed by U-Pb ages of zircons from recent river sands. *Int. J. Earth Sci.* **2014**, *103*, 579–595, doi:10.1007/s00531-013-0974-5.
3. Chmeleff, J.; von Blanckenburg, F.; Kossert, K.; Jakob, D. Determination of the ^{10}Be half-life by multicollector ICP-MS and liquid scintillation counting. *Nucl. Instr. Meth. Phys. Res. B* **2010**, *268*, 192–199, doi:10.1016/j.nimb.2009.09.012.
4. Korschinek, G.; Bergmaier, A.; Faestermann, T.; Gerstmann, U.C.; Knie, K.; Rugel, G.; Wallner, A.; Dillmann, I.; Dollinger, G.; Lierse von Gostomski, C.; et al. A new value for the half-life of ^{10}Be by Heavy-Ion Elastic Recoil Detection and liquid scintillation counting. *Nucl. Instr. Meth. Phys. Res. B* **2010**, *268*, 187–191, doi:10.1016/j.nimb.2009.09.020.
5. Norris, T.L.; Gancarz, A.J.; Rokop, D.J.; Thomas, K.W. Half-life of ^{26}Al. *J. Geophys. Res.* **1983**, *88*, B331–B333, doi:10.1029/JB088iS01p0B331.
6. Zipf, L.; Merchel, S.; Bohleber, P.; Rugel, G.; Scharf, A. Exploring ice core drilling chips from a cold Alpine glacier for cosmogenic radionuclide (^{10}Be) analysis. *Results Phys.* **2016**, *6*, 78–79, doi:10.1016/j.rinp.2016.01.002.
7. Gosse, J.C.; Phillips, F.M. Terrestrial in situ cosmogenic nuclides: Theory and application. *Quat. Sci. Rev.* **2001**, *20*, 1475–1560, doi:10.1016/S0277-3791(00)00171-2Get.
8. Balco, G.; Stone, J.O.; Lifton, N.A.; Dunai, T.J. A complete and easily accessible means of calculating surface exposure ages or erosion rates from ^{10}Be and ^{26}Al measurements. *Quat. Geochron.* **2008**, *2*, 174–195, doi:10.1016/j.quageo.2007.12.001.
9. Kutschera, W. The Half-Life of ^{14}C—Why is it so long? *Radiocarbon* **2019**, *61*, 1135–1142, doi:10.1017/RDC.2019.26.
10. Lifton, N.A.; Jull, A.J.T.; Quade, J. A new extraction technique and production rate estimate for in situ cosmogenic ^{14}C in quartz. *Geochim. Cosmochim. Acta* **2001**, *65*, 1953–1969, doi:10.1016/S0016-7037(01)00566-X.
11. Fenton, C.R.; Niedermann, S.; Dunai, T.; Binnie, S.A. The SPICE project: Production rates of cosmogenic ^{21}Ne, ^{10}Be, and ^{14}C in quartz from the 72 ka SP basalt flow, Arizona, USA. *Quat. Geochron.* **2019**, *54*, 101019, doi:10.1016/j.quageo.2019.101019.
12. Wild, E.-M.; Gauss, W.; Forstenpointner, G.; Lindblom, M.; Smetana, R.; Steier, P.; Thanheiser, U.; Weninger, F. ^{14}C dating of the Early to Late Bronze Age stratigraphic sequence of Aegina Kolonna, Greece. *NIMB* **2010**, *268*, 113–1021, doi:10.1016/j.nimb.2009.10.086.
13. Von Suchodoletz, H.; Gärtner, A.; Zielhofer, C.; Faust, D. Eemian and post-Eemian fluvial dynamics in the Lesser Caucasus. *Quat. Sci. Rev.* **2018**, *191*, 189–203, doi:10.1016/j.quascirev.2018.05.012.
14. Laronne, J.B.; Reid, I. Very high rates of bedload sediment transport by ephemeral desert rivers. *Nature* **1993**, *366*, 148–150, doi:10.1038/366148a0.
15. Ielpi, A.; Lapôtre, M.G.A.; Finotello, A.; Ghinassi, M.; D'Alpaos, A. Channel mobility drives a diverse stratigraphic architecture in the dryland Mojave River (California, USA). *Earth Surf. Proc. Landf.* **2020**, doi:10.1002/esp.4841.
16. Krapf, C.B.E.; Stollhofen, H.; Stainstreet, I.G. Contrasting styles of ephemeral river systems and their interaction with dunes of the Skeleton Coast erg (Namibia). *Quaternary Int.* **2003**, *104*, 41–52, doi:10.1016/S1040-6182(02)00134-9.

17. Bierman, P.R.; Reuter, J.M.; Pavich, M.; Gellis, A.C.; Caffee, M.W.; Larsen, J. Using cosmogenic nuclides to contrast rates of erosion and sediment yield in a semi-arid, arroyo-dominated landscape, Rio Puerco Basin, New Mexico. *Earth Surf. Proc. Landf.* **2005**, *30*, 935–953, doi:10.1002/esp.1255.
18. Binnie, S.A.; Reicherter, K.R.; Victor, P.; González, G.; Binnie, A.; Niemann, K.; Stuart, F.M.; Lenting, C.; Heinze, S.; Freeman, S.P.H.T.; et al. The origins and implications of palaeochannels in hyperarid, tectonically active regions: The northern Atacama Desert, Chile. *Glob. Planet Chang.* **2020**, *185*, 103083, doi:10.1016/j.gloplacha.2019.103083.
19. von Blanckenburg, F.; Hewawasam, T.; Kubik, P.W. Cosmogenic nuclide evidence for low weathering and denudation in wet tropical Highlands of Sri Lanka. *J. Geophys. Res.* **2004**, *109*, F03008, doi:10.1029/2003JF000049.
20. Granger, D.E.; Riebe, C.E. Cosmogenic Nuclides in Weathering and Erosion. In *Treatise on Geochemistry*, 2nd ed.; Turekian, K.; Holland, H., Eds.; Elsevier: Amsterdam, The Netherlands, 2014; pp. 401–436, doi:10.1016/B978-0-08-095975-7.00514-3.
21. Gray, H.J.; Owen, L.A.; Dietsch, C.; Beck, R.A.; Caffee, M.A.; Finkel, R.C.; Mahan, S.A. Quaternary landscape development, alluvial fan chronology and erosion of the Mecca Hills at the southern end of the San Andreas fault zone. *Quat. Sci. Rev.* **2014**, *105*, 66–85, doi:10.1016/j.quascirev.2014.09.009.
22. Hovius, N.; von Blanckenburg, F. Constraining the Denudational Response to Faulting. In *Tectonic faults: Agents of change on a dynamic Earth; Report of the 95th Dahlem Workshop on the Dynamics of Fault Zones, Berlin, 16–21 January 2005;* Handy, M., Hirth, D., Hovius, N., Eds.; MIT Press: Cambridge, MA, USA, 2007; *Dahlem Workshop Reports*; Volume 95, pp. 231–272, ISBN 978-0-2620-8362-1.
23. Aki, K. Seismic Coda Waves: A Stochastic Process in Earth's Lithosphere. In *Stochastic Models in Geosystems*; Molchanov, S.A., Woyczynski, W.A., Eds.; Springer: New York, NY, USA, 1997; *The IMA Volumes in Mathematics and its Applications*; Volume 85, pp. 1–24, ISBN 978-1-4613-8502-8.
24. Finkel, R.C.; Schaefer, J.M.; Schwartz, R. Exposure dating meets history: Precise ^{10}Be dating of very young surfaces. *Geochim. Cosmochim. Acta* **2008**, *72* (Suppl. 12), A269, doi:10.1016/j.gca.2008.05.009.
25. Schwanghart, W.; Bernhardt, A.; Stolle, A.; Hoelzmann, P.; Andermann, C.; Tofelde, S.; Merchel, S.; Rugel, G.; Fort, M.; Korup, O. Repeated catastrophic valley infill following medieval earthquakes in the Nepal Himalaya. *Science* **2016**, *351*, 147–150, doi:10.1126/science.aac9865.
26. Heineke, C.; Niedermann, S.; Hetzel, R.; Akal, C. Surface exposure dating of Holocene basalt flows and cinder cones in the Kula volcanic field (Western Turkey) using cosmogenic ^{3}He and ^{10}Be. *Quat. Geochron.* **2016**, *34*, 81–91, doi:10.1016/j.quageo.2016.04.004.
27. Bierman, P.R.; Caffee, M. Slow Rates of Rock Surface Erosion and Sediment Production across the Namib Desert and Escarpment, Southern Africa. *Am. J. Sci.* **2001**, *301*, 326–358, doi:10.2475/ajs.301.4-5.326.
28. Bierman, P.R.; Nichols, K.K.; Matmon, A.; Enzel, Y.; Larsen, J.; Finkel, R.C. 10-Be shows that Namibian drainage basins are slowly, steadily and uniformly eroding. *Quat. Intern.* **2007**, *167*, 168.
29. Miller, R.M., Namib Group. *The Geology of Namibia—Volume 3, Palaeozoic to Cenozoic*; Miller, R.G., Ed.; Ministry of Mines and Energy, Geological Survey: Windhoek, Namibia, 2008 ;pp. 25-1–25-66, ISBN 978-0-86976-733-7.
30. Hartleb, J.W.O. The Langer Heinrich Uranium Deposit: Southwest Africa/Namibia. *Ore Geol. Rev.* **1988**, *3*, 277–287, doi:10.1016/0169-1368(88)90022-4.
31. Wilkinson, M.J. *Palaeoenvironments in the Namib Desert: The lower Tumas Basin in the late Cenozoic*; University of Chicago Press: Chicago, IL, USA, 1990; *U Chicago Geogr Res Papers*, Volume 231, pp. 1–196, ISBN 0-89065-138-8.
32. Pickford, M.; Senut, B. Geology and Palaeobiology of the Namib Desert, southwestern Africa. *Mem. Geol. Surv. Namibia* **1999**, *18*, 1–155.
33. Heine, K.; Heine, J.T. A paleohydrologic reinterpretation of the Homeb Silts, Kuiseb River, central Namib Desert (Namibia) and paleoclimatic implications. *Catena* **2002**, *48*, 107–130, doi:10.1016/S0341-8162(02)00012-7.
34. Eitel. B.; Zöller, L. Die Beckensedimente von Dieprivier und Uitskot (NW-Namibia): Ein Beitrag zu ihrer paläoklimatischen Interpretation auf der Basis von Thermolumineszenzdatierungen. *Mitteilungen der Österreichischen Geographischen Gesellschaft* **1995**, *137*, 245–254.
35. Ward, J.D. The Cenozoic Succession in the Kuiseb Valley, Central Namib Desert. *Mem. Geol. Surv. S W Africa/Namibia* **1987**, *9*, 1–124.

36. Heine, K. Little Ice Age climatic fluctuations in the Namib Desert, Namibia, and adjacent areas: Evidence of exceptionally large floods from slack water deposits and desert soil sequences. In *Paleoecology of Quaternary Drylands*; Springer: Berlin, Heidelberg, 2004; Volume 102, pp. 137–165, doi:10.1007/978-3-540-44930-0_9.
37. Gray, D.R.; Foster, D.A.; Meert, J.G.; Goscombe, B.D.; Armstrong, R.; Trouw, R.A.J.; Passchier, C.W. A Damara orogen perspective on the assembly of southwestern Gondwana. *Geol. Soc. London SP* **2008**, *294*, 257–278, doi:10.1144/SP294.14.
38. Toé, W.; Vanderhaege, O.; André-Mayer, A.-S.; Feybesse, J.-L.; Milési, J.-P. From migmatites to granites in the Pan-African Damara orogenic belt, Namibia. *J. Afr. Earth. Sci.* **2013**, *85*, 62–74, doi:10.1016/j.jafrearsci.2013.04.009.
39. Zieger, J.; Harazim, S.; Hofmann, M.; Gärtner, A.; Gerdes, A.; Marko, L.; Linnemann, U. Mesozoic deposits of SW Gondwana (Namibia): Unraveling Gondwanan sedimentary dispersion drivers by detrital zircon. *Int. J. Earth Sci.* **2020**, doi:10.1007/s00531-020-01864-2.
40. Miller, R.G. Neoproterozoic and Early Palaeozoic rocks of the Damara orogen. In *The Geology of Namibia—Volume 2, Neoproterozoic to Lower Palaeozoic*. Miller, R.G., Ed.; Ministry of Mines and Energy, Geological Survey: Windhoek, Namibia, 2008; pp. 13-1–13-410, ISBN 978-0-86976-732-0.
41. Passchier, C.; Trouw, R.; da Silva Schmitt, R. How to make a transverse triple junction—New evidence for the assemblage of Gondwana along the Kaoko-Damara belts, Namibia. *Geology* **2016**, *44*, 843–846, doi:10.1130/G38015.1.
42. Greenbaum, N.; Schwartz, U.; Benito, G.; Porat, N.; Cloete, G.C.; Enzel, Y. Paleohydrology of extraordinary floods along the Swakop River at the margin of the Namib Desert and their paleoclimate implications. *Quat. Sci. Rev.* **2014**, *103*, 153–169, doi:10.1016/j.quascirev.2014.08.021.
43. Woodborne, S.; Vogel, J.C.; Collett, G. The age of sediments in the Swakop River. *Environ. Impact Assess. Propos. Khan Aquifer Recharg. Scheme* **1997**, *Appendix 5*, 1–10.
44. Ministry of Mines and Energy. *Simplified Geological Map of Namibia 1: 2000000*; Geological Survey: Windhoek, Namibia, 2000; No date, 1 sheet.
45. Steier, P.; Liebl, J.; Kutschera, W.; Wild, E.M.; Golser, R. Preparation Methods of μg Carbon Samples for ^{14}C Measurements. *Radiocarbon* **2017**, *59*, 803–814, doi:10.1017/RDC.2016.94.
46. Goodfriend, G.A. Radiocarbon age anomalies in shell carbonate of land snails from semi-arid areas. *Radiocarbon* **1987**, *29*, 159–167, doi:10.1017/S0033822200056915.
47. Merchel, S.; Gärtner, A.; Beutner, S.; Bookhagen, B.; Chabilan, A. Attempts to understand potential deficiencies in chemical procedures for AMS: Cleaning and dissolving quartz. *Nucl. Instr. Meth. Phys. Res. B* **2019**, *455*, 293–299, doi:10.1016/j.nimb.2019.02.007.
48. Merchel, S.; Arnold, M.; Aumaître, G.; Benedetti, L.; Bourlès, D.L.; Braucher, R.; Alfimov, V.; Freeman, S.P.H.T.; Steier, P.; Wallner, A. Towards more precise ^{10}Be and ^{36}Cl data from measurements at the 10^{-14} level: Influence of sample preparation. *Nucl. Instr. Meth. Phys. Res. B* **2008**, *266*, 4921–4926, doi:10.1016/j.nimb.2008.07.031.
49. Merchel, S.; Herpers, U. An update on radiochemical separation techniques for the determination of long-lived radionuclides via accelerator mass spectrometry. *Radiochim. Acta* **1999**, *84*, 215–219, doi:10.1524/ract.1999.84.4.215.
50. Akhmadaliev, S.; Heller, R.; Hanf, D.; Rugel, G.; Merchel, S. The new 6 MV AMS-facility DREAMS at Dresden. *Nucl. Instr. Meth. Phys. Res. B* **2013**, *294*, 5–10, 10.1016/j.nimb.2012.01.053.
51. Arnold, M.; Merchel, S.; Bourlès, D.L.; Braucher, R.; Benedetti, L.; Finkel, R.C.; Aumaître, G.; Gottdang, A.; Klein, M. The French accelerator mass spectrometry facility ASTER: Improved performance and developments. *Nucl. Instr. Meth. Phys. Res. B* **2010**, *268*, 1954–1959, doi:10.1016/j.nimb.2010.02.107.
52. Rugel, G.; Pavetich, S.; Akhmadaliev, S.; Enamorado Baez, S.M.; Scharf, A.; Ziegenrücker, R.; Merchel, S. The first four years of the AMS-facility DREAMS: Status and developments for more accurate radionuclide data. *Nucl. Instr. Meth. Phys. Res. B* **2016**, *370*, 94–100, doi:10.1016/j.nimb.2016.01.012.
53. Niedermann, S.; Bach, W.; Erzinger, J. Noble gas evidence for a lower mantle component in MORBs from the southern East Pacific Rise: Decoupling of He and Ne systematics. *Geochim. Cosmochim. Acta* **1997**, *61*, 2697–2715, doi:10.1016/S0016-7037(97)00102-6.
54. Hetzel, R.; Niedermann, S.; Ivy-Ochs, S.; Kubik, P.W.; Tao, M.; Gao, B. ^{21}Ne versus ^{10}Be and ^{26}Al exposure ages of fluvial terraces: The influence of crustal Ne in quartz. *Earth Planet Sci. Lett.* **2002**, *201*, 575–591, doi:10.1016/S0012-821X(02)00748-3.

55. Niedermann, S. Cosmic-ray-produced noble gases in terrestrial rocks: Dating tools for surface processes. In *Noble gases in geochemistry and cosmochemistry*; Porcelli, D., Ballentine, C.J., Wieler, R., Eds.; Mineralogical Society of America: Boulder, CO, USA, 2002; Geochemical Society; *Reviews in Mineralogy and Geochemistry* Volume 47, pp. 731–784, ISBN 978-0-9399-5059-1.
56. Niedermann, S.; Graf, T.; Marti, K. Mass spectrometric identification of cosmic-ray-produced neon in terrestrial rocks with multiple neon components. *Earth Planet Sci. Lett.* **1993**, *118*, 65–73, 10.1016/0012-821X(93)90159-7.
57. Heine, K. Holocene Climate of Namibia: A Review based on Geoarchives. *Afr. Study Monogr.* **2005**, *30*, 119–133.
58. Chase, B.M.; Meadows, M.E.; Scott, L.; Thomas, D.S.G.; Marais, E.; Sealy, J.; Reimer, P.J. A record of rapid Holocene climate change preserved in hyrax middens from southwestern Africa. *Geology* **2009**, *37*, 703–706, doi:10.1130/G30053.
59. Grodek, T.; Benito, G.; Botero, B.A.; Jacoby, Y.; Porat, N.; Haviv, I.; Cloete, G.; Enzel, Y. The last millennium largest floods in the hyperarid Kuiseb River basin, Namib Desert. *J. Quat. Sci.* **2013**, *28*, 258–270, doi:10.1002/jqs.2618.
60. Heine, K.; Völkel, J. Extreme floods around AD 1700 in the northern Namib desert, Namibia, and in the Orange River catchment, South Africa—Were they forced by a decrease of solar irradiance during the Little Ice Age? *Geogr. Pol.* **2011**, *84*, 61–80, doi:10.7163/GPol.2011.S1.5.
61. Voarintosa, N.R.G.; Brook, G.A.; Liang, F.; Marais, E.; Hardt, B.; Cheng,H.; Edwards, R.L.; Railsback, L.B. Stalagmite multi-proxy evidence of wet and dry intervals in northeastern Namibia: Linkage to latitudinal shifts of the Inter-Tropical Convergence Zone and changing solar activity from AD 1400 to 1950. *Holocene* **2016**, *27*, 384–396, doi:10.1177/0959683616660170.
62. Heyns, P.S. *Episodic Flood Events of Rivers crossing the Desert*; Episodic Events and Natural Resources Workshop: Windhoek, Namibia, 1990; 4p.
63. Brázdil, R.; Kiss, A.; Luterbacher, J.; Nash, D.J.; Řezníčková, L. Documentary data and the study of past droughts: A global state of the art. *Clim. Past* **2018**, *14*, 1915–1960, doi:10.5194/cp-14-1915-2018.
64. Borchers, B.; Marrero, S.; Balco, G.; Caffee, M.; Goehring, B.; Lifton, N.; Nishiizumi, K.; Phillips, F.; Schaefer, J.; Stone, J. Geological calibration of spallation production rates in the CRONUS-Earth project. *Quat. Geochron.* **2016**, *31*, 188–198, doi:10.1016/j.quageo.2015.01.009.
65. Stone, J.O. Air pressure and cosmogenic isotope production. *J. Geophys. Res.* **2000**, *105*, 23753–23759.
66. Braucher, R.; Merchel, S.; Borgomano, J.; Bourlès, D.L. Production of cosmogenic radionuclides at great depth: A multi element approach. *Earth Planet Sci. Lett.* **2011**, *301*, 1–9, doi:10.1016/j.epsl.2011.06.036.
67. Merchel, S., Ott, U., Herrmann, S., Spettel, B., Faestermann, T., Knie, K., Korschinek, G., Rugel, G., Wallner, A. Presolar nanodiamonds: Faster, cleaner, and limits on Platinum-HL, *Geochim. Cosmochim. Acta* **2003**, *67*, 4949–4960, doi:10.1016/S0016-7037(03)00421-6.
68. Gärtner, A.; Linnemann, U.; Hofmann, M.; Zieger, J.; Sagawe, A.; Krause, R.; Gerdes, A.; Marko, L.; Lana, C. The modern Sands of Namibia—Implications for Sedimentary Transport Processes in Southwestern Africa. In *Preparation for Submission to Quaternary Science Reviews*; ELSEVIER: Amsterdam, The Netherlands, 2020.